Materials Today Advances 31 (2026) 100872

Contents lists available at ScienceDirect

Materials Today Advances

journal homepage: www.journals.elsevier.com/materials-today-advances/

Sustainable lead-free Na_2AgSbX_6 (X = Cl, F) double perovskites with tunable optoelectronic and thermoelectric properties: A first-principles study

K. Bouferrache [a,b], M.A. Ghebouli [a,c], M. Fatmi [a,*], Faisal K. Alanazi [d], Samah Saidi [e], S. Alomairy [f], Aseel Smerat [g], Murat Yaylacı [h,i]

[a] Research Unit on Emerging Materials (RUEM), University Ferhat Abbas of Setif 1, Setif, 19000, Algeria
[b] Department of Physics, Faculty of Sciences, University of M'sila University Pole, Road Bourdj Bou Arreiridj, M'sila, 28000, Algeria
[c] Department of Chemistry, Faculty of Sciences, University of M'sila University Pole, Road Bourdj Bou Arreiridj, M'sila, 28000, Algeria
[d] Department of Physics, College of Sciences, Northern Border University, Arar, 73222, Saudi Arabia
[e] Department of Physics, College of Science and Humanities in Al-Kharj, Prince Sattam Bin Abdulaziz University, Al-Kharj, 11942, Saudi Arabia
[f] Department of Physics, College of Science, Taif University, P.O.Box 11099, Taif, 21944, Saudi Arabia
[g] Hourani Center for Applied Scientific Research, Al-Ahliyya Amman University, Amman, 19328, Jordan
[h] Department of Civil Engineering, Recep Tayyip Erdogan University, Rize, 53100, Türkiye
[i] Turgut Kıran Maritime Faculty, Recep Tayyip Erdogan University, Rize, 53900, Türkiye

ARTICLE INFO

Keywords:
Double perovskites
DFT calculations
Electronic structure
Optical properties
Thermoelectric properties
Lead-free materials

ABSTRACT

Lead-free halide double perovskites have emerged as promising candidates for sustainable energy technologies due to their low toxicity and structural stability. In this work, we investigate the structural, electronic, optical, and thermoelectric properties of Na_2AgSbX_6 (X = Cl, F) using density functional theory. Both compounds crystallize in a stable cubic Fm-3m structure, with tolerance factors (0.808–0.829) confirming their structural feasibility. The calculated indirect band gaps of 2.398 eV (Cl) and 4.11 eV (F) reveal tunable optoelectronic behavior spanning the visible to ultraviolet regions. Optical analysis demonstrates strong light absorption with low reflectivity, highlighting their suitability for photovoltaic applications. Furthermore, the compounds exhibit favorable Seebeck coefficients and promising thermoelectric performance with ZT values approaching technologically relevant ranges. The combination of environmental compatibility, tunable electronic structure, and multifunctional energy conversion capabilities positions Na_2AgSbX_6 double perovskites as attractive candidates for next-generation sustainable photovoltaic and thermoelectric devices.

1. Introduction

Halide double perovskites are promising alternatives to lead-based perovskites such as $MAPbI_3$ because they offer good optoelectronic properties, lower toxicity, better stability, and cost-effective synthesis. Consequently, research has shifted toward developing lead-free alternatives with enhanced thermal, structural, and environmental stability. Among these alternatives, the compound Na_2AgSbX_6 (X = Cl, F) has emerged as a promising candidate. It exhibits favorable thermodynamic and mechanical stability, with negative formation energies, indirect band gaps in the solar spectrum range, and ZT values approaching 1, indicating its potential for energy conversion applications [1]. Its bismuth-based analogue $Na_2AgBiBr_6$ has also demonstrated a suitable band gap (~2.6 eV), strong light absorption, and a thermoelectric performance factor ZT ≈ 0.77, reinforcing its utility in photovoltaic and thermoelectric applications [2]. Studies on the Cs_2AgBX_6 family (B = In, Sb; X = F, Cl, Br, I) reveal cubic perovskite structures with balanced electron and hole effective masses and band gaps ranging from visible to UV regions, making them suitable for high-efficiency optoelectronic devices [3]. Furthermore, mesoporous single crystals of $Cs_2AgBiBr_6$ prepared using infrared-assisted spin-coating techniques have shown enhanced solar cell efficiency (from 0.28% to 0.86%) due to increased light scattering and surface area [4]. $Cs_2AgBiBr_6$ single crystals also display high resistivity (~10^9–10^{10} Ω cm), indirect band gaps (~2.1 eV), and excellent photo-response to X-ray radiation, positioning them as reliable candidates for photodetectors and radiation sensors [5].

* Corresponding author.
E-mail address: m.fatmi@univ-setif.dz (M. Fatmi).

https://doi.org/10.1016/j.mtadv.2026.100872
Received 15 May 2026; Received in revised form 14 June 2026; Accepted 22 June 2026
Available online 27 June 2026

Comparatively, $Cs_2AgBiCl_6$ exhibits higher mechanical and thermal stability with better resistance to environmental degradation, making it more suitable for robust energy devices [6]. Other halide double perovskites such as $X_2GeSnCl_6$ (X = Na, K) have demonstrated direct band gaps (~2.2 eV), strong visible absorption, and low reflectivity, along with high thermoelectric efficiency (ZT ≈ 1), marking them as dual-purpose materials for solar and thermal energy harvesting [7]. Rb_2AgBiI_6 has been synthesized for the first time as a thin film, showing thermal stability up to 440°C and a direct band gap (~1.98 eV), suitable for low-cost solar cell fabrication [8]. Likewise, $Cs_2AgInCl_6$ and $Cs_2AgInBr_6$ have shown direct band gaps (2.61 eV and 1.68 eV, respectively), high absorption in the visible spectrum, and high Seebeck coefficients with increasing electrical conductivity, confirming their potential for next-generation thermoelectric devices [9]. Another group of Na-based double perovskites, Na_2CuMX_6 (M = Sb, Bi; X = Cl, Br), was found to possess cubic structures, direct band gaps in the visible range, strong optical absorption, and excellent charge transport, making them strong candidates for sustainable energy applications [10]. Most recently, DFT-based investigations on Rb_2TlSbX_6 (X = Cl, Br, I) have shown highly stable perovskite structures with direct band gaps between 1.04 and 2.07 eV, high Seebeck coefficients, and ultralow thermal conductivity. These features lead to thermoelectric figures of merit (ZT) exceeding 1.9, alongside strong visible light absorption and low reflectivity, positioning these compounds at the forefront of high-performance optoelectronic and thermoelectric materials [11]. Recent studies have also emphasized that the practical performance of perovskite and optoelectronic materials is not determined only by the band-gap value, but also by device stability, hysteresis behavior, interface/passivation engineering, defect control, carrier localization, charge transport, and long-term operation. For example, passivation layers in degraded 2D–3D perovskite solar cells were shown to reduce hysteresis and degradation effects, which are critical for practical photovoltaic performance [12]. Defect passivation has also been reported as an effective strategy to improve transport stability in functional electronic materials [13]. In addition, heterostructure engineering can enhance charge-transfer behavior and energy-conversion performance [14], while carrier localization and minority-carrier lifetime strongly influence the optical response of advanced optoelectronic heterostructures [15]. These studies indicate that a realistic assessment of new lead-free perovskite-inspired materials should combine electronic, optical, thermal, mechanical, and transport-related descriptors rather than relying only on band-gap values. Recent developments in perovskite and double-perovskite materials further demonstrate the importance of combining structural, electronic, optical, mechanical, and thermoelectric descriptors when evaluating materials for energy-related technologies. For example, Ba_3NX_3 (X = F, Cl) halide perovskites have been reported to exhibit direct band gaps, strong optical absorption, and promising thermoelectric performance, with ZT values reaching 1.23 for Ba_3NF_3 and 0.90 for Ba_3NCl_3 at 700 K [16]. Similarly, copper-based double perovskites Rb_2YCuX_6 (X = Br, I) were shown to possess stable cubic structures, suitable semiconducting band gaps, high optical absorption in the visible/near-visible range, and promising optoelectronic and thermoelectric behavior [17]. Experimental studies on Mg-doped Sr_2FeNbO_6 double perovskites also confirmed that doping can tune the band gap, optical response, dielectric behavior, and structural stability, which is important for advanced optoelectronic and wireless applications [18]. Moreover, lead-free Ca_2MnMoO_6 double perovskite has been reported as a mechanically stable material with strong optical absorption and promising spintronic/optoelectronic potential [19]. These recent studies highlight that the current challenge is not only to identify lead-free perovskites with suitable band gaps, but also to evaluate their stability, optical response, mechanical behavior, and transport-related properties in a unified framework. Accordingly, the present work focuses on $Na_2AgSbCl_6$ and Na_2AgSbF_6 and investigates their structural, electronic, optical, elastic, thermodynamic, phonon, and thermoelectric properties using first-principles calculations. It should be noted that Na_2AgSbX_6 (X = F, Cl, Br, I) compounds have already been investigated in a previous theoretical study, where structural, electronic, optical, thermodynamic, mechanical, phonon, and thermoelectric properties were reported. Therefore, the present work is not claimed as the first study of this family. Instead, it provides a focused reassessment of the Cl- and F-based compounds using an internally consistent DFT framework, with emphasis on mBJ-GGA-based electronic and optical interpretation, elastic anisotropy analysis, phonon-supported stability, thermodynamic behavior, and a more cautious classification of their realistic application domains [20]. A systematic comparison between the two cations configurations is maintained throughout, and the calculated results are discussed in relation to available experimental observations and previous theoretical studies. More broadly, the reliability of first-principles calculations for predicting physical properties has been demonstrated across different families of functional materials. For example, DFT-based approaches have been successfully applied to doped semiconductors to predict magnetic, optical, and thermoelectric behavior [21], and to fluorite mixed oxides for evaluating structural, electronic, mechanical, and optical properties [22]. Similar first-principles strategies have also been used for spinel oxide ceramics and $BaTiO_3$-based systems, where structural stability, optical response, and thermoelectric trends were investigated [23,24]. In addition, Heusler alloys and organic semiconductors have been studied using DFT to understand magnetic, optoelectronic, and composition-dependent electronic behavior [25,26]. Related lead-free halide double perovskites, such as Na_2AgBiX_6 (X = Br, Cl), have also been investigated using first-principles calculations to assess structural, elastic, electronic, and optical properties [27]. Therefore, although the present work is computational, it follows a well-established predictive strategy that has been successfully applied to diverse materials systems. Recent first-principles studies have further emphasized the growing interest in lead-free double perovskites and related perovskite-like materials for energy applications. Mądra-Gackowska et al. investigated A_2BBiCl_6 (A = Cs, K; B = Ag, Au) halide double perovskites and demonstrated their structural, dynamical, optoelectronic, mechanical, and thermodynamic relevance for next-generation photovoltaic applications [28]. Szeleszczuk et al. reported a combined optoelectronic and thermoelectric analysis of X_2YBiCl_6 (X = Cs, Na; Y = Ag, Au) double perovskites, highlighting the role of cation modification in tuning visible-light absorption and thermoelectric response [29]. In addition, DFT-based studies on X_3NI_3 (X = Sr, Ba) halide perovskites have shown that band-gap modulation can improve thermoelectric response [30]. Cubic X_2YInO_6 (X = Ba, Sr; Y = Nb, V) double perovskites have also been investigated for their coupled optoelectronic and thermoelectric performance [31]. Furthermore, Sr_2MReO_6 (M = Li, Na, K) double perovskites demonstrate that cation tuning is an effective strategy for controlling electronic and thermoelectric behavior [32]. Although Na_2AgSbX_6 compounds have been previously reported, the present work extends earlier studies by providing a combined analysis of structural, phonon, electronic, optical, elastic anisotropy, thermodynamic, and thermoelectric properties within one consistent DFT framework. This comprehensive approach allows a clearer evaluation of the realistic potential of $Na_2AgSbCl_6$ for visible/near-UV optoelectronic and thermoelectric applications, and Na_2AgSbF_6 for wide-band-gap UV-related and thermally robust applications.

2. Computational methods

First-principles calculations were carried out using the WIEN2k package [33], which is based on the FP-LAPW method within density functional theory. The exchange–correlation effects were described using both PBE-GGA and the modified Becke–Johnson potential [34,35], with the latter used to obtain more reliable semiconductor band gaps. This choice is motivated by the well-known limitation of standard semilocal functionals such as PBE-GGA, which usually underestimate the experimental band gaps of semiconductors and halide perovskites due to self-interaction errors and the lack of derivative discontinuity in

the exchange–correlation potential [36]. Therefore, the mBJ-GGA potential was employed to obtain a more reliable estimation of the electronic band gaps and the related optical response, while keeping a reasonable computational cost compared with hybrid functional. The muffin-tin radii were selected as 2.5 a.u. for Na, Ag, and Sb, 2.30 a.u. for Cl, and 1.95 a.u. for F, while the cutoff parameter was fixed at RMT×Kmax = 9.0. Brillouin-zone integrations were performed using 1000 k-points for structural and electronic calculations, 10000 k-points for optical and thermoelectric properties, and 5000 k-points for elastic properties [37]. The convergence criteria were set to 10^{-4} Ry for total energy and 10^{-3} e for charge. Optical properties were obtained through the optic module within the random phase approximation, whereas thermoelectric coefficients were calculated using BoltzTraP under the constant relaxation time approximation over 300–900 K [38]. Finally, phonon dispersions were computed with PHONOPY using the finite displacement method and WIEN2k forces to verify the dynamical stability [39].

3. Results and discussion

3.1. Structural properties

The Na_2AgSbX_6 (X = Cl, F) compounds crystallize in the cubic double perovskite (Fm-3m). Fig. 1 shows the schematic crystal structure, where Na^+ cations occupy the A-sites, while Ag^+ and Sb^{3+} cations alternately occupy the B-sites in an ordered arrangement, surrounded by X^- anions forming octahedral coordination.

The crystal structures were optimized by fitting the energy–volume data to the Birch–Murnaghan equation of state to obtain the equilibrium parameters [40].

$$E(V)-E(V_0)=\frac{B_0V}{B_0'}\left[\frac{(V_0/V)^{B_0'}}{B_0'-1}+1\right]-\frac{B_0V_0}{B_0'-1} \quad (1)$$

$$B=V\frac{\partial^2E}{\partial V^2}=\frac{4}{9a}\frac{\partial^2E}{\partial a^2} \quad (2)$$

$$B_0'=\partial B/\partial P \quad (3)$$

The structural optimization results are presented in Table 1 and Fig. 2. The calculated equilibrium lattice parameters are 10.673 Å for $Na_2AgSbCl_6$ and 9.181 Å for Na_2AgSbF_6. These values show excellent agreement with previous theoretical calculations, with deviations of less than 0.5%. The smaller lattice parameter for the fluoride compound is consistent with the smaller ionic radius of F^- compared to Cl^-.The bulk moduli are calculated to be 29.005 GPa and 47.584 GPa for $Na_2AgSbCl_6$ and Na_2AgSbF_6, respectively. The higher bulk modulus of the fluoride compound indicates stronger bonding and reduced compressibility, which is attributed to the higher electronegativity and smaller size of fluorine.

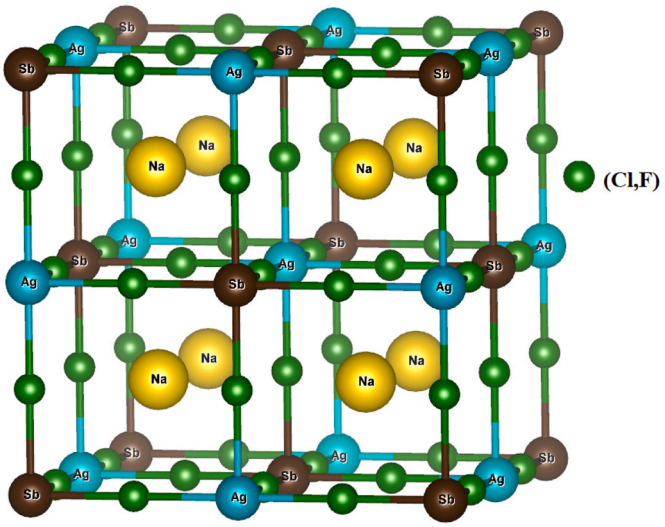

Fig. 1. Schematic crystal structure ofNa_2AgSbX_6(X = Cl, F).

Table 1
Thermodynamics parameters of Na_2AgSbX_6 (X = Cl, F).

	a_0(Ang)	B(GPa)	B'	E_0(Ry)
$Na_2AgSbCl_6$	10.673	29.005	5.463	−29790.404882
	10.648[1]	29.856[1]	4.855[1]	−29790.378[1]
Na_2AgSbF_6	9.181	47.584	4.972	−25450.7377
	9.056[1]	52.693[1]	4.776[1]	−25450.646[1]

The structural stability of double perovskites can be assessed using the Goldschmidt tolerance factor (t) and octahedral factor (μ). The calculated values are presented in Table 2. For $Na_2AgSbCl_6$, t = 0.808 and μ = 0.522, while for Na_2AgSbF_6, t = 0.829 and μ = 0.710. These values fall within the acceptable range for stable perovskite structures ($0.8 < t < 1.0$ and $0.4 < \mu < 0.7$), confirming the structural stability of both compounds. However, the octahedral factor of Na_2AgSbF_6 (μ = 0.710) is slightly above the commonly accepted upper limit of 0.70 and should therefore be interpreted as very close to, rather than strictly within, the ideal range. This slight deviation may indicate reduced ideal octahedral compatibility or a possible tendency toward structural distortion; however, the optimized cubic structure, elastic stability criteria, and phonon results support its computational stability.

Although the tolerance factor and octahedral factor provide useful preliminary indicators of structural feasibility, they are not sufficient alone to confirm the stability of double perovskite compounds. Therefore, additional stability criteria were considered in the present work. The calculated formation energies were used as thermodynamic stability indicators, while the elastic constants were used to evaluate mechanical stability according to the Born stability criteria. In addition, phonon dispersion calculations were performed to further examine the dynamical stability of $Na_2AgSbCl_6$ and Na_2AgSbF_6. Therefore, the stability of the studied compounds is discussed based on combined structural, thermodynamic, mechanical, and dynamical criteria rather than on the tolerance factor alone.

To further clarify the origin of structural differences between $Na_2AgSbCl_6$ and Na_2AgSbF_6, the ionic radii of the substituted halide ions are considered. The ionic radius of Cl^- (1.81 Å) is significantly larger than that of F^- (1.33 Å). This reduction in ionic size leads to lattice contraction in Na_2AgSbF_6, as observed in Table 1. The smaller F^- ion enhances electrostatic interactions and strengthens the B–X bonding framework, which is consistent with the higher bulk modulus and reduced compressibility of the fluoride compound. However, this size mismatch also slightly affects the ideal octahedral coordination environment, contributing to a mild structural distortion reflected in the octahedral factor value. Overall, halide substitution plays a key role in tuning lattice parameters, bond strength, and elastic response in these double perovskites. Fig. 3; presents the phonon dispersion curves of $Na_2AgSbCl_6$ and Na_2AgSbF_6 along the selected high-symmetry directions in the Brillouin zone. The phonon spectra reveal the presence of a few imaginary phonon branches near specific symmetry points, indicating a degree of dynamical instability in the ideal cubic phase at 0 K. Such soft phonon modes are commonly associated with octahedral tilting, lattice distortions, or possible symmetry-lowering structural transitions. Similar behavior has been reported for Na_2AgSbX_6 (X = F, Cl, Br, and I) double perovskites by Kumari et al. [20], where imaginary phonon modes were also observed and attributed to lattice instabilities in the cubic structure. Despite these soft modes, the optimized structures satisfy the structural and mechanical stability criteria and may be stabilized at finite temperatures through anharmonic lattice effects. Therefore, the present phonon results suggest that the ideal cubic phase is mechanically stable but exhibits signatures of dynamical instability

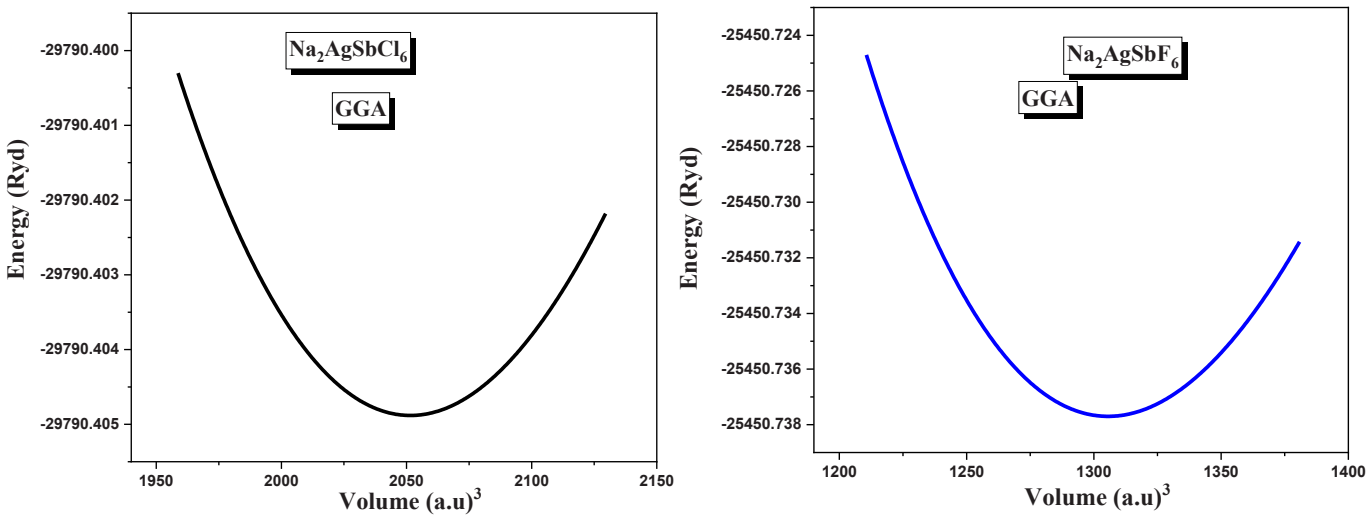

Fig. 2. Energy vs. volume curves for $Na_2AgSbCl_6$ and Na_2AgSbF_6 using GGA approximation.

Table 2
Goldschmidt tolerance factor (t) and octahedral factor (μ) for Na_2AgSbX_6(X = Cl, F).

	t-factor	μ-factor
$Na_2AgSbCl_6$	0.808	0.522
Na_2AgSbF_6	0.829	0.710

that may drive structural distortions under certain conditions.

3.2. Electronic properties

The electronic band structures calculated using the mBJ-GGA functional are shown in Fig. 4. Both compounds exhibit indirect semiconductor behavior with the valence band maximum (VBM) located at the Γ point and the conduction band minimum (CBM) at different k-points along the Brillouin zone. The calculated band gaps are significantly different between the two compounds: 2.398 eV for $Na_2AgSbCl_6$ and 4.11 eV for Na_2AgSbF_6 (Table 3).

The nature of the band gap has been carefully confirmed from the electronic band structures, where the VBM is located at the Γ point while the CBM appears at different k-points in the Brillouin zone. This clearly confirms that both $Na_2AgSbCl_6$ and Na_2AgSbF_6 exhibit indirect band gap behavior. This substantial difference is primarily attributed to the different electronegativities and ionic radii of the halogen atoms. The larger band gap of the fluoride compound makes it more suitable for UV applications, while the chloride compound with its smaller band gap is better suited for visible light applications. However, due to the indirect nature of the band gap and the relatively large value of 2.398 eV, $Na_2AgSbCl_6$ should be considered more cautiously as a visible/near-UV optoelectronic material rather than an ideal single-junction photovoltaic absorber. In contrast, the wide band gap of Na_2AgSbF_6 confirms its more realistic suitability for UV-related and wide-band-gap applications. The total and partial density of states (DOS) are presented in Fig. 4. The analysis reveals that the valence band is primarily composed of halogen p-states and Ag d-states, while the conduction band is dominated by Sb p-states with some contribution from halogen s-states. The sharp peaks in the DOS near the Fermi level indicate strong localization of electronic states, which is characteristic of ionic compounds. For $Na_2AgSbCl_6$, the valence band shows significant contribution from Cl 3p states hybridized with Ag 4d states, while for Na_2AgSbF_6, the F 2p states dominate the valence band. The conduction band in both compounds is primarily composed of Sb 5p states, indicating that the optical transitions are mainly from halogen p-states to Sb p-states. To further assess the reliability of the electronic structure, spin–orbit coupling (SOC) effects were also considered by comparing GGA, mBJ, and mBJ + SOC calculations. The results show that SOC slightly reduces the band-gap values for both compounds due to relativistic effects associated with Sb and Ag atoms. However, SOC does not significantly alter the band dispersion, nor does it change the positions of the VBM and CBM, indicating that the overall electronic nature remains preserved.

Furthermore, comparison with the HSE06 functional shows good

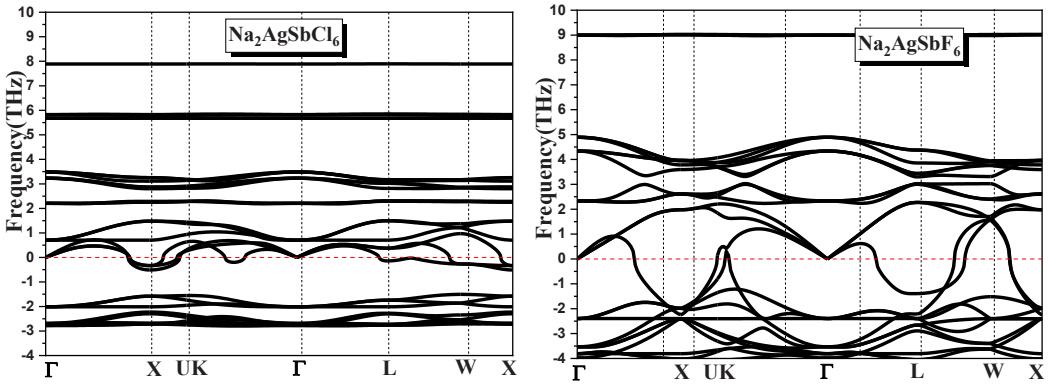

Fig. 3. Phonon dispersion curves of $Na_2AgSbCl_6$ and Na_2AgSbF_6.

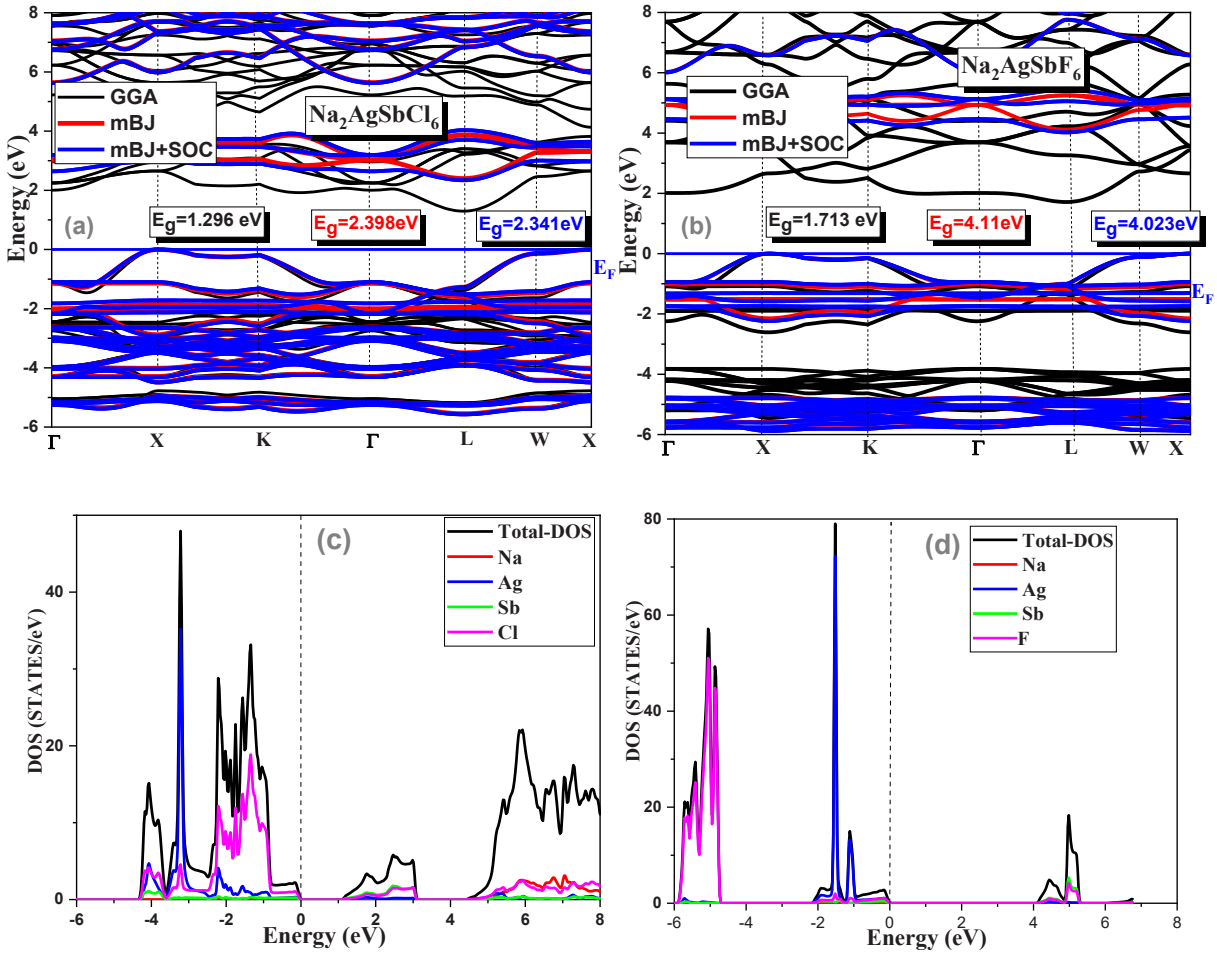

Fig. 4. Electronic properties of Na_2AgSbX_6 (X = Cl, F): (a,b) electronic band structures and (c,d) total and partial density of states calculated using the mBJ-GGA approach.

Table 3
Calculated band-gap energies (eV) of Na_2AgSbX_6 (X = Cl, F) obtained using GGA, mBJ, mBJ + SOC, and HSE06 functionals.

	GGA	mBJ	mBJ + SO	HSE06
$Na_2AgSbCl_6$	1.296	2.398 2.212[41] 2.833[1]	2.341	1.269
Na_2AgSbF_6	1.713	4.11 3.986[1]	4.023	3.019

agreement with the mBJ trends, confirming the reliability of the calculated band-gap values. Small differences between GGA, mBJ, mBJ + SOC, and HSE06 are expected due to the different treatments of exchange–correlation effects.

3.3. Elastic properties

The elastic constants show that Na_2AgSbF_6 has higher values (C_{11} = 93.539 GPa) compared to $Na_2AgSbCl_6$ (C_{11} = 57.31 GPa), indicating stronger resistance to deformation along the crystallographic axes. The relatively large increase in C_{11} for Na_2AgSbF_6 was carefully verified and can be attributed to the smaller ionic radius and higher electronegativity of fluorine compared with chlorine, which strengthen the interatomic interactions and increase the rigidity of the crystal lattice. Similar trends relating stronger bonding interactions to enhanced elastic stiffness have been reported in previous first-principles investigations of functional materials and intermetallic compounds [42–44]. The calculated bulk moduli (B_H) are 28.711 GPa and 47.857 GPa for the Cl and F compounds, respectively, confirming the higher incompressibility of the fluoride compound. The shear moduli (G_H) are 10.234 GPa and 12.653 GPa, respectively, indicating moderate resistance to shear deformation. The anisotropy factors (A) are 0.276 and 0.160 for the Cl and F compounds, respectively. Values significantly different from 1 indicate elastic anisotropy, with the chloride compound showing higher anisotropy.For $Na_2AgSbCl_6$, the values are E_V = 31.904 GPa, E_R = 22.801 GPa, and E_H = 27.442 GPa. The fluoride compound shows higher values: E_V = 45.627 GPa, E_R = 23.527 GPa, and E_H = 34.885 GPa. The Hill average provides the most reliable estimate of the Young's modulus, indicating that Na_2AgSbF_6 has approximately 27% higher stiffness than $Na_2AgSbCl_6$.The significant difference between the Voigt and Reuss bounds indicates elastic anisotropy in both compounds, with the chloride compound showing greater anisotropy (ΔE = 9.103 GPa vs. 22.1 GPa for the fluoride).The Poisson's ratio (ν) provides insight into the lateral contraction when a material is stretched. For $Na_2AgSbCl_6$, the calculated values are ν_V = 0.315, ν_R = 0.368, and ν_H = 0.341. The fluoride compound shows higher values: ν_V = 0.341, ν_R = 0.418, and ν_H = 0.379 (Table 4).The Poisson's ratio values for both compounds are in the typical range for ionic materials (0.2-0.4), indicating normal lateral deformation behavior. The higher Poisson's ratio of Na_2AgSbF_6 suggests greater lateral contraction upon stretching, which is consistent with its more ionic character due to the higher electronegativity of fluorine. The Pugh's ratio (B_H/G_H) is a key indicator of ductility versus brittleness. The calculated ratios are 2.805 and 3.782 for

Table 4
Summary of the elastic and mechanical characteristics of Na_2AgSbX_6 (X = Cl, F).

	$Na_2AgSbCl_6$	Na_2AgSbF_6
C_{11} (GPa)	57.31	93.539
C_{12} (GPa)	14.412	25.016
C_{44} (GPa)	5.922	5.511
G_v (GPa)	12.133	17.011
G_R (GPa)	8.336	8.295
G_H (GPa)	10.234	12.653
B_H (GPa)	28.711	47.857
A	0.276	0.160
E_V (GPa)	31.904	45.627
E_R (GPa)	22.801	23.527
E_H (GPa)	27.442	34.885
ϑ_V	0.315	0.341
ϑ_R	0.368	0.418
ϑ_H	0.341	0.379
B_H/G_H	2.805	3.782
The average wave velocity (m/s)	2199.548	2195.569
Debye Temperature(K)	209.823	243.493

$Na_2AgSbCl_6$ and Na_2AgSbF_6, respectively. Since both values are greater than the critical value of 1.75, both compounds exhibit ductile behavior, which is beneficial for practical applications and processing. The higher B_H/G_H ratio of the fluoride compound (3.782) indicates greater ductility compared to the chloride compound (2.805). This enhanced ductility is advantageous for manufacturing processes and mechanical reliability in device applications. The mechanical behavior observed for $Na_2AgSbCl_6$ and Na_2AgSbF_6 is consistent with previous first-principles investigations on functional materials, where the fulfillment of the Born mechanical stability criteria and Pugh's ratio values exceeding 1.75 were associated with mechanically stable and ductile compounds. Similar methodologies have been successfully applied to cubic perovskites, Heusler alloys, and intermetallic systems to evaluate elastic stiffness, structural robustness, and mechanical reliability under external perturbations [42–44]. The present results therefore further support the mechanical stability and potential technological applicability of the studied double perovskites.

The Debye temperature θ_D can be defined as the temperature at which all the atomic modes of vibrations in a solid become activated. At low temperatures, θ_D can be calculated from the speed of velocity v_m as follows [45]:

$$\theta_D = \frac{h}{k_B}\left[\left(\frac{3n}{4\pi}\right)\frac{N_A\rho}{M}\right]^{1/3} v_m \tag{4}$$

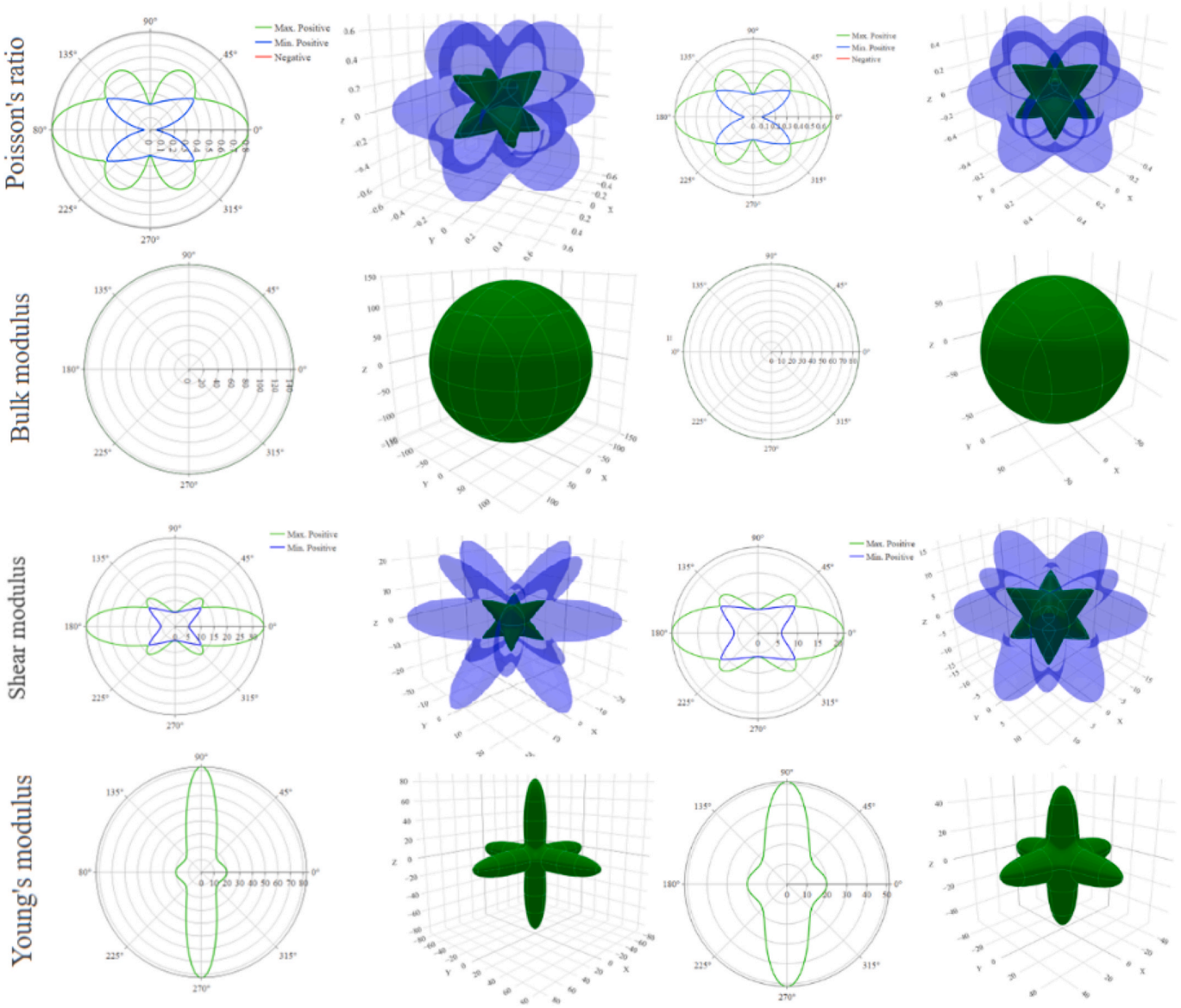

Fig. 5. Configuration of elastic moduli in 2D and 3D forms for Na_2AgSbX_6 (X = Cl, F).

In the expression of equation (4), the quantities h, n, ρ, k_B, M and N_A denote: the Planck constant; the number of atoms in the unit cell, the density of the solid, the Boltzmann constant, the molar mass of the solid and the Avogadro number, respectively.

The values are 209.823 K for $Na_2AgSbCl_6$ and 243.493 K for Na_2AgSbF_6. The higher Debye temperature of Na_2AgSbF_6 suggests stronger bonding and a higher characteristic phonon frequency compared with $Na_2AgSbCl_6$. The average wave velocity was calculated to be 2199.548 m/s and 2195.569 m/s for $Na_2AgSbCl_6$ and Na_2AgSbF_6, respectively. The similar values indicate comparable acoustic properties despite the different Debye temperatures. Fig. 5 presents the three-dimensional and two-dimensional representations of the elastic moduli for both compounds, providing valuable insights into the anisotropic behavior of these materials. For $Na_2AgSbCl_6$, the 3D representation shows significant deviations from spherical symmetry, indicating pronounced elastic anisotropy. The Young's modulus varies considerably with crystallographic direction, with maximum values along certain high-symmetry directions and minimum values along others.

The non-spherical shape of the 3D surface confirms the anisotropic nature of the material, consistent with the calculated Zener anisotropy factors. Since an isotropic material has A = 1, any deviation from unity indicates elastic anisotropy. The calculated values of A = 0.276 for $Na_2AgSbCl_6$ and A = 0.160 for Na_2AgSbF_6 indicate that both compounds are elastically anisotropic, with Na_2AgSbF_6 showing stronger anisotropy according to the Zener criterion because its value is farther from unity. Therefore, the comparison between the two compounds should be based on their deviation from A = 1 rather than on the apparent smoothness of the 3D elastic surface alone. Fig. 5 confirms the directional dependence of the elastic moduli, with $Na_2AgSbCl_6$ showing stronger anisotropic behavior, whereas Na_2AgSbF_6 exhibits relatively smoother directional variation. The shear modulus representations reveal that both compounds have relatively low shear resistance, consistent with their ductile nature. The 3D surfaces for shear moduli show similar anisotropic patterns to the Young's modulus, with the chloride compound exhibiting greater directional variation.

These visualizations are particularly important for understanding: i. The directional dependence guides the selection of optimal crystallographic orientations for specific mechanical applications. ii. The degree of anisotropy affects the mechanical properties of polycrystalline samples. iii. Anisotropic materials may develop stress concentrations along certain directions under mechanical loading.

The more isotropic behavior of Na_2AgSbF_6 makes it potentially more suitable for applications where uniform mechanical properties are desired, while the anisotropic nature of $Na_2AgSbCl_6$ could be

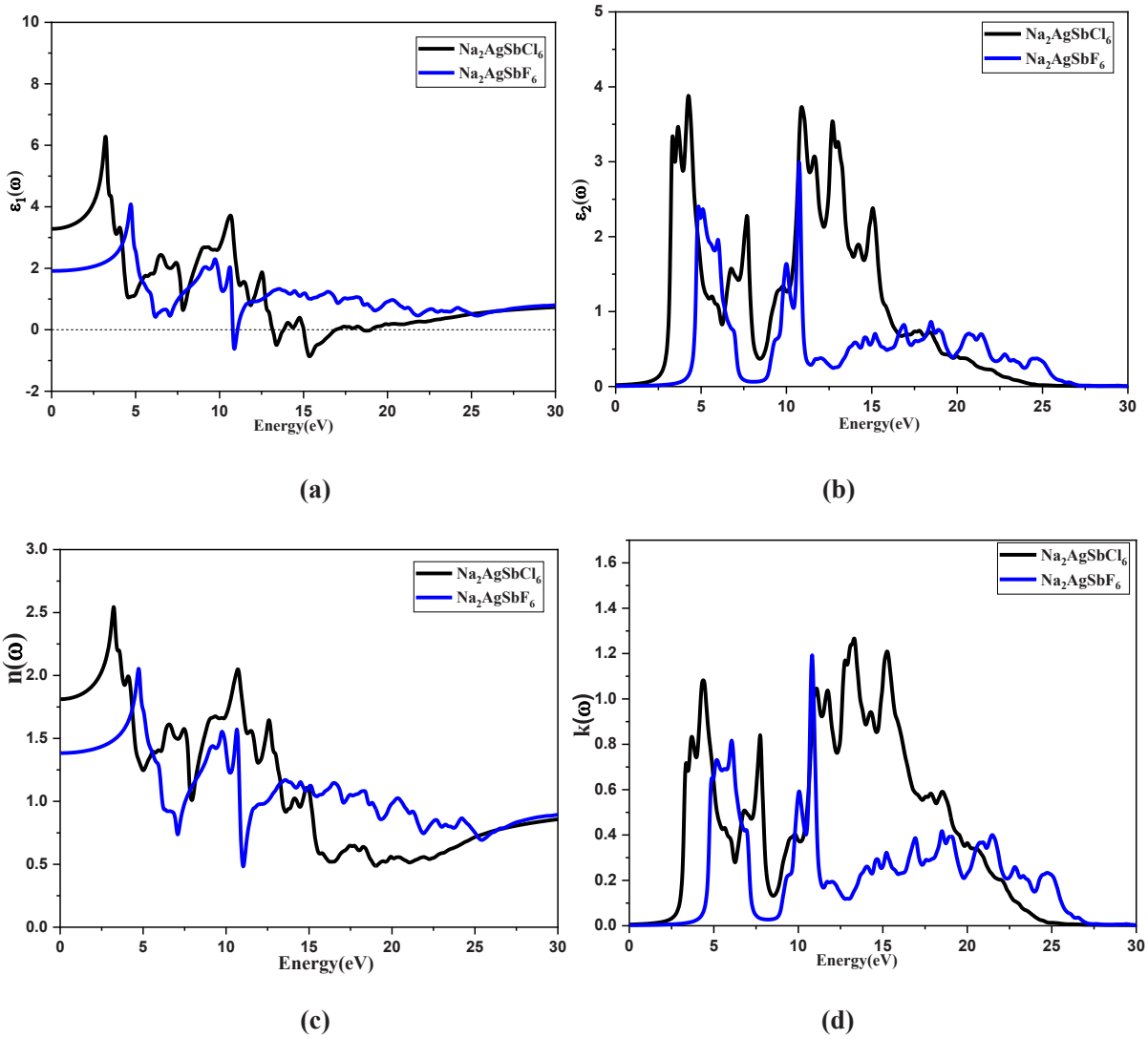

Fig. 6. Optical spectra of Na_2AgSbX_6 (X = Cl, F) calculated using the mBJ-GGA approach: (a) real part of the dielectric function $\varepsilon_1(\omega)$, (b) imaginary part of the dielectric function $\varepsilon_2(\omega)$, (c) refractive index n(ω), (d) extinction coefficient k(ω), (e) energy-loss function L(ω), (f) absorption coefficient α(ω), (g) optical conductivity σ(ω), and (h) reflectivity R(ω) as a function of photon energy.

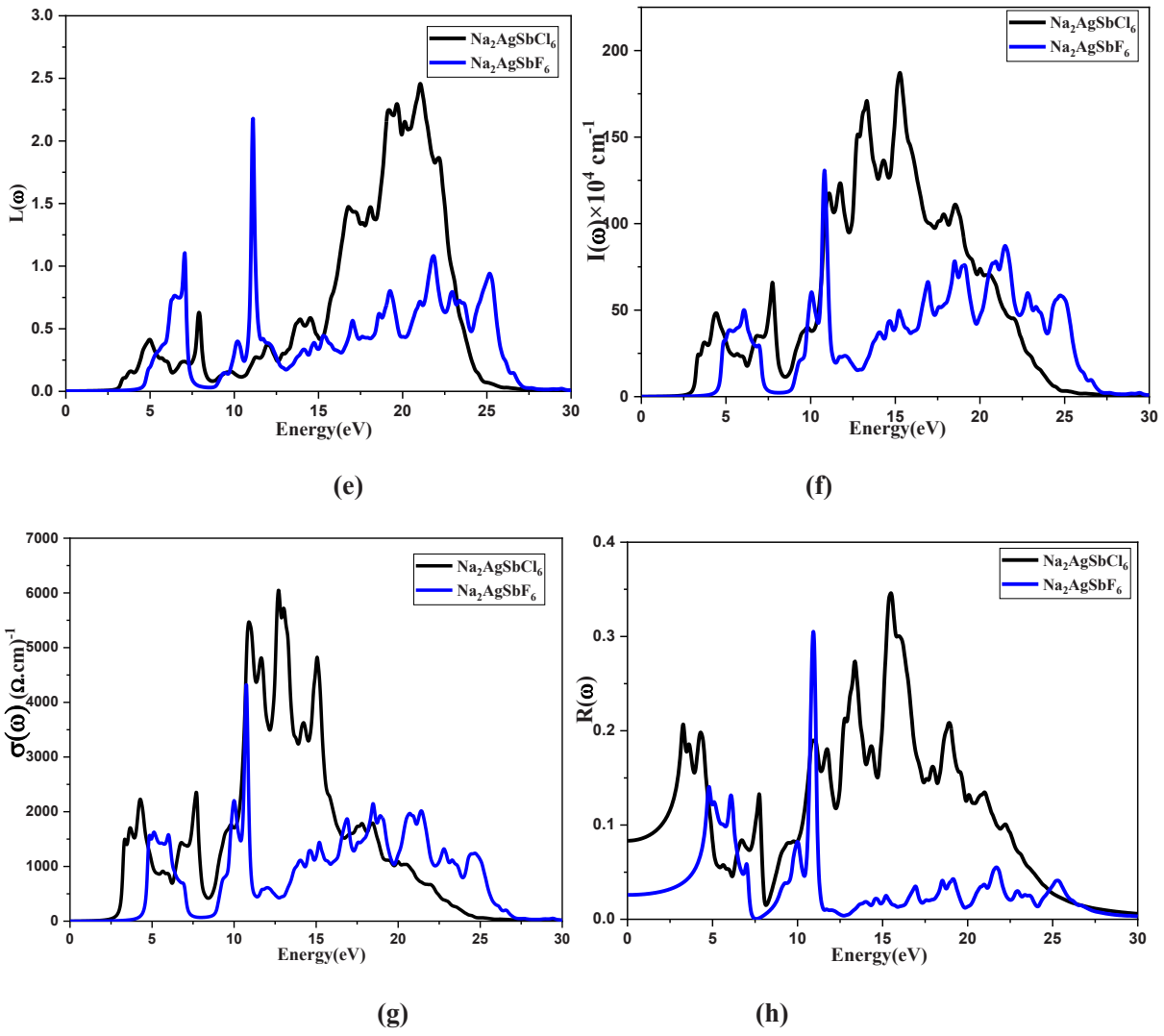

Fig. 6. (*continued*).

advantageous for applications requiring directional mechanical properties.

3.4. Optical properties

Using the mBJ-GGA functional for accurate band-gap estimation, the frequency-dependent optical functions are shown in Fig. 6. The real part of the dielectric function $\varepsilon_1(\omega)$ shows static dielectric constants of 3.282 for $Na_2AgSbCl_6$ and 1.913 for Na_2AgSbF_6, with the lower value of the fluoride compound being consistent with its wider band gap and stronger ionic character (Table 5). The imaginary part indicates that optical absorption for $Na_2AgSbCl_6$ begins around 2.4 eV, matching the fundamental band gap and exhibiting multiple peaks in the visible and UV regions due to various interband transitions, whereas for Na_2AgSbF_6 the onset occurs at about 4.1 eV, restricting absorption to the UV range.

Table 5
Calculated static dielectric constant $\varepsilon(0)$and, static refractive index and static optical reflectivity for of Na_2AgSbX_6 (X = Cl, F).

	$\varepsilon(0)$	n(0)	R(0)
$Na_2AgSbCl_6$	3.282	1.811	0.083
	5.327[1]	2.346[1]	0.479[1]
Na_2AgSbF_6	1.913	1.383	0.025
	3.713[1]	1.974[1]	0.549[1]

The static refractive indices are 1.811 and 1.383 for the chloride and fluoride compounds, respectively, with the higher value for $Na_2AgSbCl_6$ attributed to its smaller band gap and greater polarizability. Reflectivity spectra reveal relatively low reflectivity values of 0.083 for $Na_2AgSbCl_6$ and 0.025 for Na_2AgSbF_6, indicating limited optical losses at low photon energies. The absorption coefficient α(ω) reaches 10^4–10^5 cm^{-1}, with $Na_2AgSbCl_6$ absorbing mainly in the visible/near-UV region and Na_2AgSbF_6 being mainly active in the UV range.

Nevertheless, the photovoltaic interpretation should be considered with caution. The indirect band gap of $Na_2AgSbCl_6$ and its absorption onset around 2.4 eV make it less suitable as a primary single-junction solar absorber compared with lower-gap direct semiconductors. Therefore, $Na_2AgSbCl_6$ may be more realistically described as a visible/near-UV optoelectronic or complementary absorber material. On the other hand, Na_2AgSbF_6, with a band gap above 4 eV and absorption mainly in the UV region, is better suited for UV photodetectors, transparent/window-layer applications, and wide-band-gap optoelectronic devices rather than conventional photovoltaic absorbers.

3.5. Thermoelectric properties

The thermoelectric properties, calculated using the BoltzTraP code and shown in Fig. 7, reveal temperature-dependent transport behaviors that underline the potential of these materials for thermoelectric

applications.

The Seebeck coefficient S(T) displays both positive and negative values depending on carrier type and temperature, ranging from −200 to +400 μV/K for $Na_2AgSbCl_6$ between 300 and 800 K, with the sign change suggesting the feasibility of both n-type and p-type conduction under suitable doping. Na_2AgSbF_6 generally exhibits larger absolute values, reaching up to 600 μV/K, a result of its wider band gap and lower carrier concentration. The electrical conductivity σ(T) decreases with temperature for both compounds, characteristic of semiconductors, with $Na_2AgSbCl_6$ showing higher values due to its smaller band gap, while Na_2AgSbF_6 remains lower in line with its insulating character. Thermal conductivity consists of electronic (κ_e) and lattice (κ_e) components; κ_e follows the Wiedemann–Franz law and scales with σ(T), whereas κ_e is lower for $Na_2AgSbCl_6$ due to stronger phonon scattering from heavier Cl atoms. The thermoelectric figure of merit $ZT = S^2\sigma T/\kappa$ reaches peak values of about 0.8 for $Na_2AgSbCl_6$ and 0.6 for Na_2AgSbF_6 at high temperatures, indicating moderate yet promising thermoelectric performance, particularly with optimized doping strategies. It should be noted that these thermoelectric results were obtained within the constant relaxation time approximation as implemented in BoltzTraP. Therefore, the electrical conductivity and electronic thermal conductivity should be interpreted as σ/τ and κ_e/τ, respectively, rather than

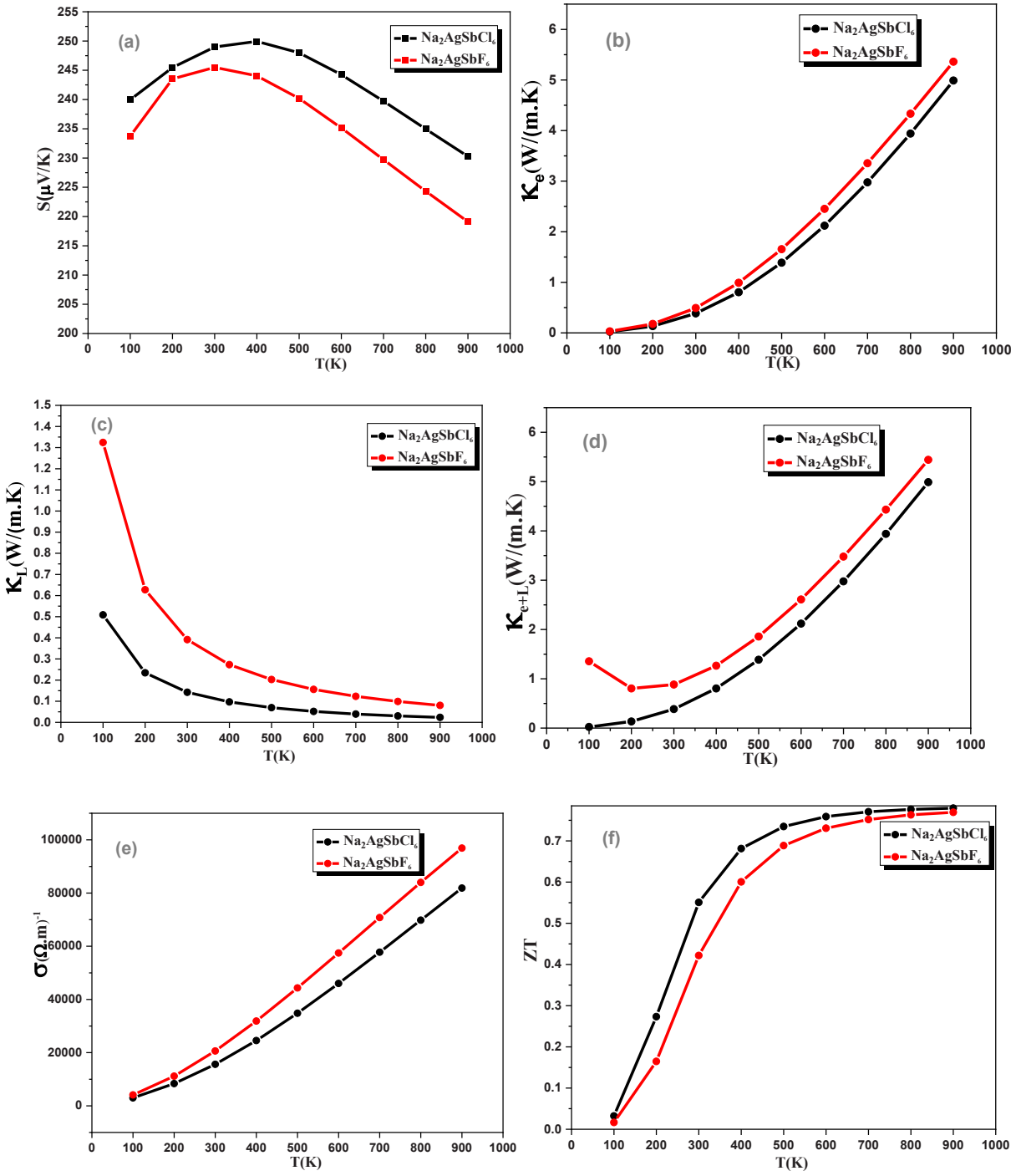

Fig. 7. Temperature dependence of thermoelectric transport properties: (a) Seebeck coefficient, (b) electronic thermal conductivity, (c) lattice thermal conductivity, (d) total thermal conductivity, (e) electrical conductivity, and (f) thermoelectric figure of merit (ZT) for Na_2AgSbX_6 (X = Cl, F) perovskites using the mBJ-GGA approximation.

absolute values unless a specific relaxation time is assumed. In the present work, the lattice thermal conductivity κ_e was estimated using a semi-empirical relation based on the Debye temperature and related elastic/thermodynamic parameters, rather than from a full phonon Boltzmann transport treatment [46]. Consequently, the reported ZT values should be regarded as indicative estimates and comparative trends rather than definitive absolute thermoelectric figures of merit. A more rigorous assessment of thermoelectric performance would require explicit carrier-concentration optimization, relaxation-time evaluation, and full phonon-transport-based lattice thermal conductivity calculations.

3.6. Thermodynamic properties

The thermodynamic properties of Na_2AgSbX_6 (X = Cl, F), obtained using the quasi-harmonic approximation, are shown in Figs. 8 and 9 as functions of temperature and pressure.

These results include heat capacity, entropy, Debye temperature, and thermal expansion coefficient, with C_v and Cp approaching the Dulong–Petit limit at high temperatures. The Debye temperatures are 209.823 K for $Na_2AgSbCl_6$ and 243.493 K for Na_2AgSbF_6, the higher value for the fluoride reflecting stronger interatomic bonding and higher phonon frequencies associated with the smaller and more electronegative F atoms. The thermal expansion coefficient α(T) rises with temperature for both materials, with values typical of ionic solids; the

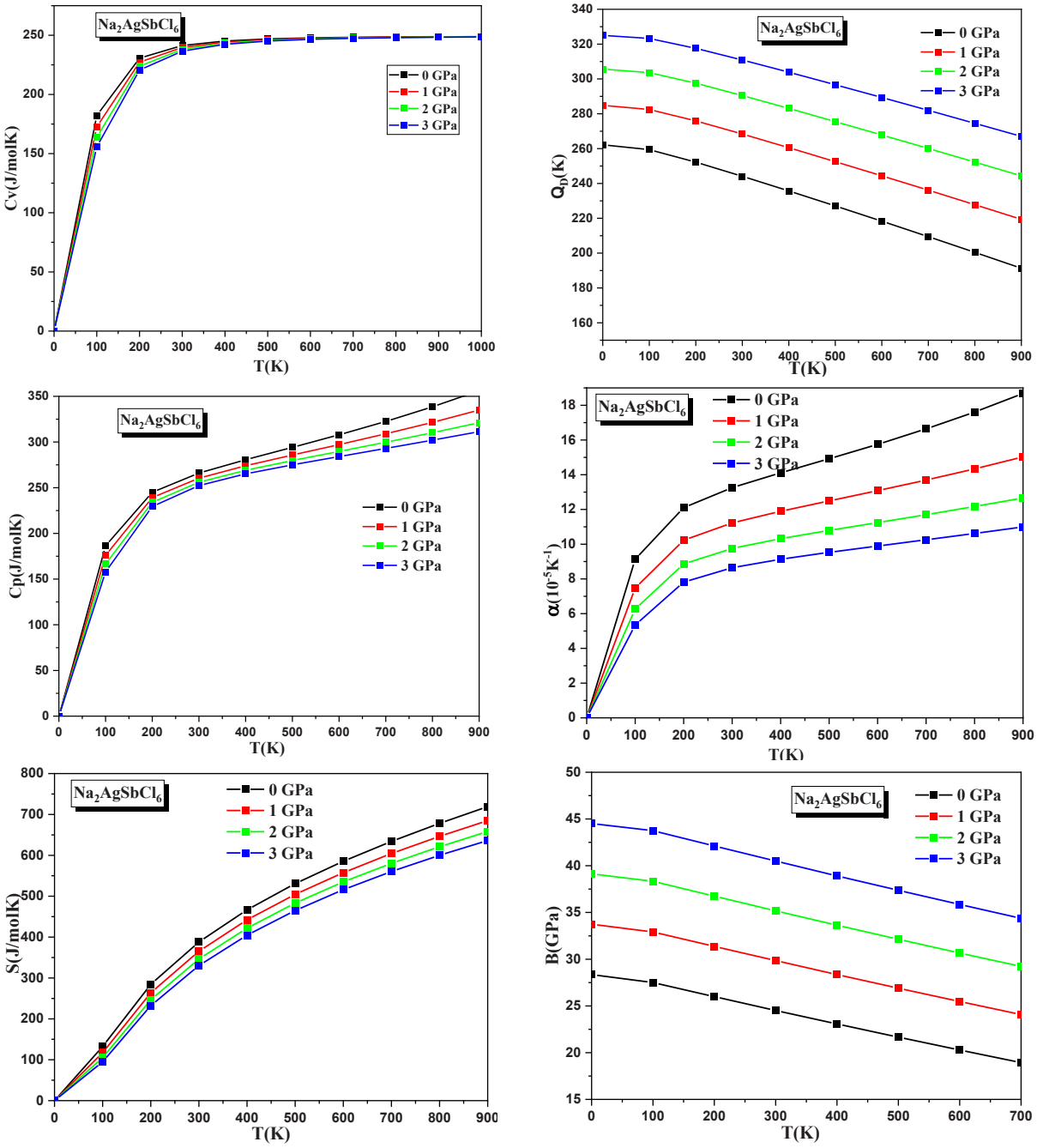

Fig. 8. Temperature-dependent thermodynamic properties of $Na_2AgSbCl_6$ at different pressures, including C_v, Cp, entropy, Debye temperature, and thermal expansion coefficient, calculated using GGA.

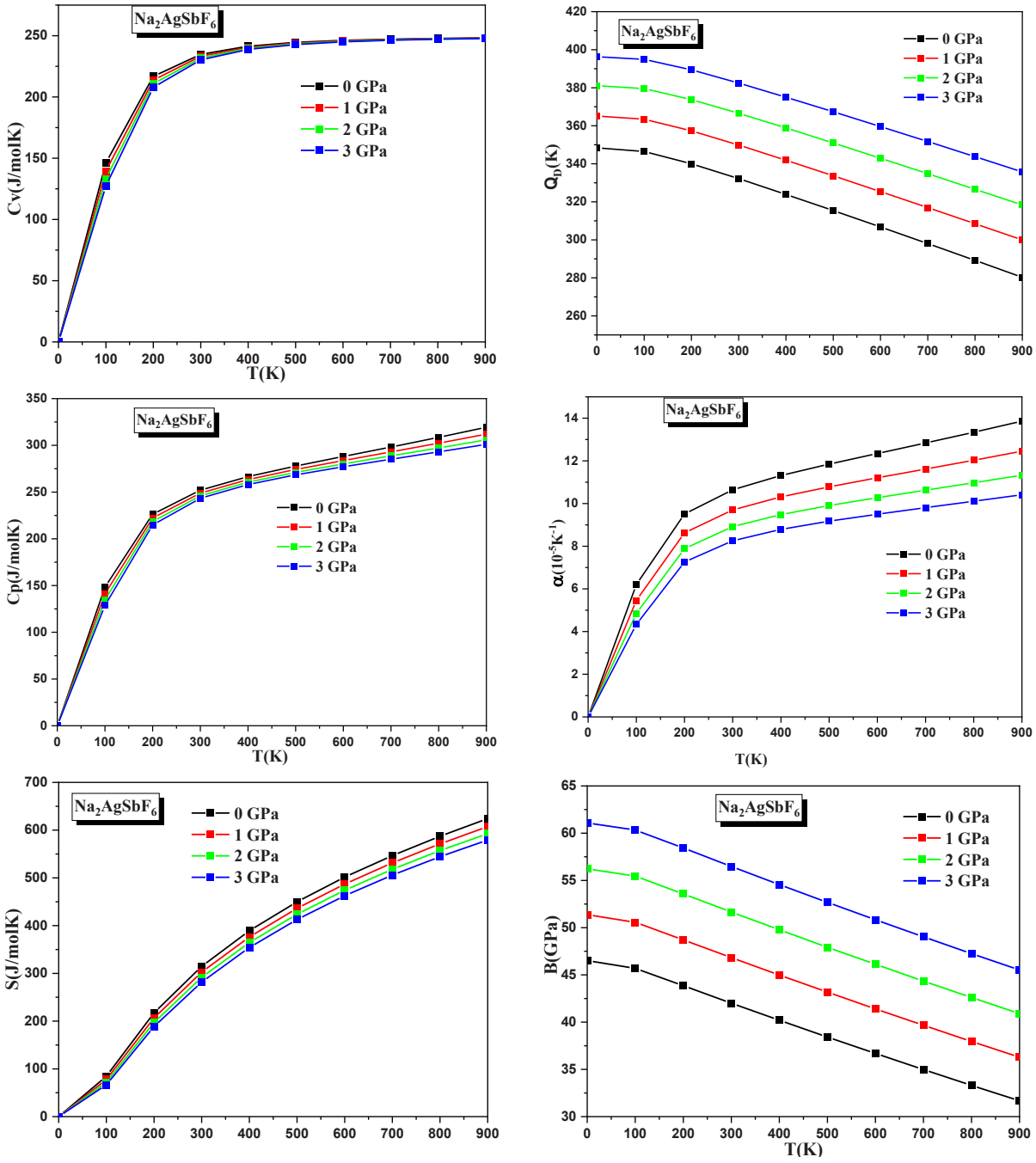

Fig. 9. Temperature-dependent thermodynamic properties of Na_2AgSbF_6 under various pressures, including C_v, Cp, entropy, Debye temperature, and thermal expansion coefficient, calculated using GGA.

chloride compound exhibits slightly higher expansion, consistent with its weaker bonding.

3.7. Comparison with related perovskite systems and limitations

To further place the present results in context, a comparison with related lead-free double perovskites and perovskite-like systems is useful. Previous studies on Cs_2AgBiX_6 (X = Br, Cl) reported indirect band-gap behavior and visible-light optical response, while also emphasizing that indirect-gap double perovskites should be considered carefully for photovoltaic applications [47]. This is consistent with the present interpretation of $Na_2AgSbCl_6$, which exhibits visible/near-UV absorption but should not be regarded as an ideal single-junction photovoltaic absorber due to its indirect band gap. Similarly, recent investigations on Sb-based halide double perovskites such as $K_2AgSbBr_6$ and its doped derivatives have shown that compositional modification can strongly tune the band gap and optical absorption, confirming that halide and cation chemistry play a key role in controlling optoelectronic functionality [48].

Recent DFT studies on Au-, In-, As-, and transition-metal-based double perovskites further confirm that the optoelectronic and thermoelectric responses of these materials are strongly composition-dependent. For example, $Rb_2AsAuBr_6$ and $Rb_2AsAuCl_6$ have been investigated as multifunctional double perovskites combining optoelectronic and thermoelectric behavior [49], while $Cs_2InAgBr_6$ and $Cs_2InAgCl_6$ have been reported as lead-free double perovskites with

coupled optical and thermoelectric potential [50]. In comparison, the present Na_2AgSbX_6 compounds show a more application-dependent behavior. $Na_2AgSbCl_6$ is more relevant for visible/near-UV optoelectronic and thermoelectric-related applications, whereas Na_2AgSbF_6, because of its wide band gap of 4.11 eV and UV-dominated absorption, is better described as a wide-band-gap UV-related material.

Related DFT studies on Rb_2LiAsX_6 (X = F, Cl, Br, I) double perovskites also demonstrate that the optical response shifts systematically with halide substitution, supporting the present trend observed between the Cl- and F-based compounds [51]. Moreover, studies on K_2CuVCl_6 and Rb_2CuVCl_6 have shown that double perovskite frameworks can be tuned toward spintronic, optoelectronic, and energy-related functionalities through cation selection and electronic-structure engineering [52]. Additional theoretical investigations on oxide double perovskites such as Sr_2AlXO_6 (X = Ta, Nb, V) and Cs_2CaMCl_6 (M = Ge, Pb) further support the usefulness of first-principles calculations for predicting structural, elastic, electronic, optical, phonon, thermoelectric, and thermodynamic trends in related perovskite families [53,54]. It should be emphasized, however, that the present study remains computational. In the absence of direct experimental synthesis and device-level measurements for $Na_2AgSbCl_6$ and Na_2AgSbF_6, the predicted properties should be viewed as theoretical indicators rather than definitive performance metrics. Further experimental validation, synthesis feasibility assessment, carrier-transport measurements, and more advanced phonon-transport calculations are required to confirm their practical applicability.

4. Conclusions

We have presented a comprehensive first-principles investigation of the lead-free double perovskites Na_2AgSbX_6 (X = Cl, F) using state-of-the-art computational methods. Our key findings can be summarized as follows:

1. Both compounds exhibit structural feasibility and mechanical stability indicators in the cubic double perovskite structure, as confirmed by the Goldschmidt tolerance factors and octahedral factors within or close to the acceptable ranges.
2. The materials are indirect semiconductors with band gaps of 2.398 eV ($Na_2AgSbCl_6$) and 4.11 eV (Na_2AgSbF_6), making them suitable for different optical applications. The electronic structure analysis reveals that optical transitions are primarily from halogen p-states to Sb p-states.
3. The elastic constants confirm mechanical stability, with both compounds showing ductile behavior. The fluoride compound exhibits higher mechanical strength and lower compressibility than the chloride compound.
4. Strong optical absorption in the visible and UV regions application-dependent optoelectronic potential rather than universal photovoltaic suitability. $Na_2AgSbCl_6$ shows superior visible light absorption, while Na_2AgSbF_6 is more suitable for UV applications.
5. Both compounds show moderate thermoelectric behavior with significant Seebeck coefficients and indicative figures of merit. The temperature-dependent transport properties suggest potential for thermoelectric applications, particularly with appropriate doping optimization, although more rigorous transport calculations are required for quantitative performance assessment.
6. The comprehensive thermodynamic analysis demonstrates favorable thermal response over a wide temperature range, with the fluoride compound showing higher Debye temperature and stronger interatomic bonding.

Overall, the present results indicate that Na_2AgSbX_6 double perovskites are computationally promising lead-free materials with application-dependent optoelectronic, thermal, and thermoelectric features. However, further experimental validation and more advanced stability and transport calculations are required to assess their practical device performance.

CRediT authorship contribution statement

K. Bouferrache: Conceptualization. **M.A. Ghebouli:** Formal analysis. **M. Fatmi:** Formal analysis, Validation. **Faisal K. Alanazi:** Formal analysis. **Samah Saidi:** Formal analysis. **S. Alomairy:** Data curation. **Aseel Smerat:** Resources. **Murat Yaylacı:** Investigation.

Declaration of competing interest

The authors declare that they have no known competing financial interests or personal relationships that could have appeared to influence the work reported in this paper.

Acknowledgements

The authors extend their appreciation to the Deanship of Scientific Research at Northern Border University, Arar, KSA for funding this research work through the project number NBUFFR-2026-310-04.

Data availability

No data was used for the research described in the article.

References

[1] S. Kumari, K.P. Kamlesh, L. Kumari, S. Kumar, S. Kumari, R. Singh, R. Gupta, M. S. Chauhan, U. Rani, A.S. Verma, Progress in theoretical study of lead-free halide double perovskite Na_2AgSbX_6 (X = F, Cl, Br, and I) thermoelectric materials, J. Mol. Model. 29 (6) (2023) 195, https://doi.org/10.1007/s00894-023-05599-0.

[2] A. Ayyaz, G. Murtaza, A. Usman, H. Alkhaldi, M.Q. Shah, S. Ali, N. Sfina, M. Younas, M. Irfan, Structural, morphological, elastic, optoelectronic and thermoelectric properties of lead-free double perovskite $Na_2AgBiBr_6$ for photovoltaic applications: experimental and DFT insight, Ceram. Int. 50 (9A) (2024) 15261–15272, https://doi.org/10.1016/j.ceramint.2024.02.002.

[3] C.-J. Yu, et al., First-principles study on structural, electronic and optical properties of halide double perovskite Cs_2AgBX_6 (B = In, Sb; X = F, Cl, Br, I), RSC Adv. 13 (2023) 24541–24551, https://doi.org/10.1039/D3RA02566G.

[4] S.P. Maurya, et al., $Cs_2AgBiBr_6$ and related halide double perovskite porous single crystals, Sci. Rep. 15 (2025) 4202, https://doi.org/10.1038/s41598-025-11939-z.

[5] V. Murgulov, C. Schweinle, M. Daub, et al., Double perovskite $Cs_2AgBiBr_6$ radiation sensor: synthesis and characterization of single crystals, J. Mater. Sci. 57 (2022) 2758–2774, https://doi.org/10.1007/s10853-021-06847-5.

[6] M.A. Ghebouli, K. Bouferrache, R. Boudissa, et al., Exploring the mechanical, dynamical, and thermal stability of Cs_2AgBiX_6 (X = Br, Cl) for optoelectronic and thermoelectric applications, Sci. Rep. 15 (2025) 20993, https://doi.org/10.1038/s41598-025-05549-1.

[7] M. Shafiq, M.Q. Shah, G. Murtaza, et al., Ab initio study of lead-free double halide perovskite $X_2GeSnCl_6$ (X = Na, K) compounds for energy conversion system, Arabian J. Sci. Eng. 49 (2024) 10061–10074, https://doi.org/10.1007/s13369-024-08751-x.

[8] A. Bhorde, et al., Structural, electronic, and optical properties of lead-free halide double perovskite Rb_2AgBiI_6: a combined experimental and density functional theory study, ES Mater. Manuf. 12 (2021) 43–52, https://doi.org/10.30919/esmm5f1042.

[9] M. Fatmi, et al., High performance double perovskites of $Cs_2InAgBr_6$ and $Cs_2InAgCl_6$ for future thermoelectric and solar cell applications: a DFT study, Sci. Rep. 15 (2025) 4869, https://doi.org/10.1038/s41598-025-04600-5.

[10] A. Ayyaz, G. Murtaza, M. Umer, A. Usman, H.H. Raza, Structural, elastic, optoelectronic, and transport properties of Na-based halide double perovskites Na_2CuMX_6 (M = Sb, Bi, and X = Cl, Br) as renewable energy materials: a DFT insight, Sci. Rep. 14 (2024) 15564, https://doi.org/10.1557/s43578-023-01181-9.

[11] T.S. Ahmad, et al., Optoelectronic and thermoelectric analysis of halide stable double perovskite Rb_2TlSbX_6 (X = Cl, Br, I) via DFT calculations, Results Phys. 63 (2024) 107885, https://doi.org/10.1016/j.rinp.2024.107885.

[12] V.E. Ledesma-García, J.J. Rodríguez-Pérez, M. Reta-Hernández, J.M. Rivas, M. Medina-Llamas, I. Zarazúa, S.H. Turren-Cruz, D. Esparza, Hysteresis and capacitance effects on degraded 2D–3D perovskite solar cells with passivation layers, Sol. Energy 302 (2025) 114070, https://doi.org/10.1016/j.solener.2025.114070.

[13] J. Qi, K. Tie, Y. Ma, Y. Huang, W. Gong, S. Sun, Z. Wang, Z. Li, R. Huang, J. Bi, L. Li, X. Chen, W. Hu, Achieving zero-temperature coefficient point behavior by defect passivation for temperature-immune organic field-effect transistors, Adv. Mater. 36 (2024) 2400089, https://doi.org/10.1002/adma.202400089.

[14] J. Zhang, X. Wang, M. Zhong, J. Cao, Z. Shi, B. Su, Z. Lei, Se-doped Co_9S_8/Ni_3S_2 heterostructure nanowires as self-supported catalysts for alkaline oxygen evolution, J. Alloys Compd. 1039 (2025) 183096, https://doi.org/10.1016/j.jallcom.2025.183096.

[15] Y. Hao, Z. Su, W. Li, X. Fang, D. Wang, D. Fang, J. Li, S. Xu, P. Du, Characteristics of carrier localization and their effects on minority carrier lifetime in InAs/$In_{0.5}Ga_{0.5}As_{0.5}Sb_{0.5}$ type-II superlattices, Appl. Phys. Lett. 127 (2025) 082105, https://doi.org/10.1063/5.0273175.

[16] A.M. Alsuhaibani, F. Rehman, M. Liaqat, A.M. Quraishi, M. Norberdiyewa, A. Ullah, I. Khan, V. Tirth, R.M. Mohammed, A. Alqahtani, M.S. Refat, A. Zaman, High thermoelectric and opto-electronic properties of Ba_3NX_3 (X = F, Cl) perovskite: insights from DFT computation, Radiat. Phys. Chem. 225 (2024) 112129, https://doi.org/10.1016/j.radphyschem.2024.112129.

[17] F. Rehman, N. Elboughdiri, I. Sherazov, A.M. Quraishi, O. Mohsen, V. Tirth, A. Alqahtani, H. Alqahtani, R.M. Mohammed, A.M. Alsuhaibani, M.S. Refat, N.M. A. Hadia, A. Zaman, Exploring the structural, electronic, optical, mechanical and thermoelectric properties of copper based double perovskites Rb_2YCuX_6 (X = Br, I), J. Phys. Chem. Solid. 196 (2025) 112382, https://doi.org/10.1016/j.jpcs.2024.112382.

[18] A. Ullah, F. Ullah, K. Ullah, F. Rehman, A. Alhodidi, S.H. Alrefaee, S.K. Knani, V. Tirth, A. Alqahtani, A. Zaman, Exploration of the structural, optical, and dielectric performance of Mg-doped Sr_2FeNbO_6 double perovskite for wireless applications, Electrochem. Commun. 177 (2025) 107981, https://doi.org/10.1016/j.elecom.2025.107981.

[19] S. H. Alrefaee Shazia, A. Kumar, H. Karamti, N. Mukhtar, N. Ismaylova, N. Akhter, F. Rehman, V. Tirth, A. Alqahtani, A. Zaman, Structural, mechanical and optical properties of lead-free ferromagnetic Ca_2MnMoO_6 double perovskite for advanced optoelectronic applications, Chem. Phys. 600 (2026) 112911, https://doi.org/10.1016/j.chemphys.2025.112911.

[20] S. Kumari, P.K. Kamlesh, L. Kumari, et al., Progress in theoretical study of lead-free halide double perovskite Na_2AgSbX_6 (X = F, Cl, Br, and I) thermoelectric materials, J. Mol. Model. 29 (2023) 195, https://doi.org/10.1007/s00894-023-05599-0.

[21] F.A. Bensaber, B. Amiri, B. Bouabdallah, I. Bouchama, S. Alomairy, M.A. Ghebouli, M. Fatmi, B. Ghebouli, M.J.A. Abualreish, A. Smerat, The potential of Tm-Doped GaN: a comprehensive study of magnetic, optical, and thermoelectric properties for optoelectronic and energy conversion applications, J. Supercond. Nov. Magnetism 39 (2026) 81, https://doi.org/10.1007/s10948-026-07176-x.

[22] K. Bouferrache, M.A. Ghebouli, S. Saidi, M. Fatmi, M.J.A. Abualreish, A. Smerat, M. Yaylacı, S. Alomairy, Structural, electronic, mechanical and optical properties of $Pu_{1-x}Th_xO_2$ fluorite ceramics: a first-principles study, Mater. Today Commun. 53 (2026) 115356, https://doi.org/10.1016/j.mtcomm.2026.115356.

[23] K. Bouferrache, M.A. Ghebouli, M. Fatmi, B. Ghebouli, F.K. Alanazi, M.J. A. Abualreish, A. Smerat, M. Yaylacı, First-principles insights into structural, elastic, electronic, optical, and thermoelectric properties of $ZnRh_2O_4$ spinel oxide ceramic, J. Korean Ceram. Soc. (2026), https://doi.org/10.1007/s43207-026-00616-3.

[24] M.A. Ghebouli, K. Bouferrache, S. Alomairy, N. Bioud, M. Fatmi, B. Ghebouli, T. M. Althagafi, M.J.A. Abualreish, Structural, optical and thermoelectric characterization of $BaTiO_3$ for solar, sensor and photonic applications, Semiconductors 60 (2026) 61–78, https://doi.org/10.1134/S1063782625603115.

[25] K. Bouferrache, M.A. Ghebouli, Y. Slimani, B. Ghebouli, M. Fatmi, T. Chihi, N. Algethami, S.A. Mouhammad, S. Alomairy, E.B. Elkenany, Structural stability, opto-electronic, magnetic and thermoelectric properties of half-metallic ferromagnets quaternary Heusler alloys CoFeXAs (X = Mn, Cr and V), Solid State Commun. 377 (2024) 115366, https://doi.org/10.1016/j.ssc.2023.115366.

[26] F. Benlakhdar, M.A. Ghebouli, M. Fatmi, B. Ghebouli, S. Alomairy, F.K. Alanazi, A. Djemli, T.M. Althagafi, Effect of halogen substitution on the electronic and optical behavior of $C_{16}H_{10}X_2O_2$ (X = F, Cl, Br and I) organic semiconductors, Sci. Rep. 15 (2025) 25891, https://doi.org/10.1038/s41598-025-11846-6.

[27] M.A. Ghebouli, T. Chihi, B. Ghebouli, M. Fatmi, Study of the structural, elastic, electronic and optical properties of lead free halide double perovskites Cs_2AgBiX_6 (X = Br, Cl), Chin. J. Phys. 56 (2018) 323–330, https://doi.org/10.1016/j.cjph.2018.01.004.

[28] K. Mądra-Gackowska, M. Gackowski, Ł. Szeleszczuk, Density functional theory insights into A_2BBiCl_6 (A = Cs, K; B = Ag, Au) halide double perovskites for next-generation photovoltaics, Phys. B Condens. Matter 726 (2026) 418286, https://doi.org/10.1016/j.physb.2026.418286.

[29] Ł. Szeleszczuk, K. Mądra-Gackowska, V.B. Hacholli, M. Gackowski, Designing efficient energy materials: optoelectronic and thermoelectric perspectives of X_2YBiCl_6 (X = Cs, Na; Y = Ag, Au) double perovskites, J. Phys. Chem. Solid. 209 (2026) 113293, https://doi.org/10.1016/j.jpcs.2025.113293.

[30] Ł. Szeleszczuk, K. Mądra-Gackowska, M. Gackowski, Exploring band gap modulation and thermoelectric excellence in X_3NI_3 (X = Sr, Ba) halide perovskites, Physica Scripta 101 (2026) 125902, https://doi.org/10.1088/1402-4896/ae515c.

[31] Ł. Szeleszczuk, K. Mądra-Gackowska, M. Gackowski, Optoelectronic and thermoelectric performance of cubic X_2YInO_6 (X = Ba, Sr; Y = Nb, V) double perovskites: a first-principles approach, Phys. B Condens. Matter 719 (2025) 417958, https://doi.org/10.1016/j.physb.2025.417958.

[32] M. Gackowski, K. Mądra-Gackowska, Ł. Szeleszczuk, Cation-tuned electronic and thermoelectric properties in Sr_2MReO_6 (M = Li, Na, K) double perovskites: a first-principles perspective, Opt. Quant. Electron. 58 (2026) 241, https://doi.org/10.1007/s11082-026-08837-w.

[33] P. Blaha, K. Schwarz, G.K.H. Madsen, D. Kvasnicka, J. Luitz, WIEN2k: an Augmented Plane Wave plus Local Orbitals Program for Calculating Crystal Properties, Vienna University of Technology, Vienna, Austria, 2001.

[34] J.P. Perdew, K. Burke, M. Ernzerhof, Generalized gradient approximation made simple, Phys. Rev. Lett. 77 (18) (1996) 3865–3868, https://doi.org/10.1103/PhysRevLett.77.3865.

[35] A.D. Becke, E.R. Johnson, A simple effective potential for exchange, J. Chem. Phys. 124 (2006) 221101, https://doi.org/10.1063/1.2213970.

[36] B. Ghebouli, M.A. Ghebouli, T. Chihi, M. Fatmi, S. Boucetta, M. Reffas, First-principles study of structural, elastic, electronic and optical properties of $SrMO_3$ (M = Ti and Sn), Solid State Commun. 149 (47–48) (2009) 2244–2249, https://doi.org/10.1016/j.ssc.2009.09.001.

[37] H.J. Monkhorst, J.D. Pack, Special points for Brillouin-zone integrations, Phys. Rev. B 13 (1976) 5188–5192, https://doi.org/10.1103/PhysRevB.13.5188.

[38] G.K.H. Madsen, D.J. Singh, BoltzTraP. A code for calculating band-structure dependent quantities, Comput. Phys. Commun. 175 (1) (2006) 67–71, https://doi.org/10.1016/j.cpc.2006.03.007.

[39] A. Togo, I. Tanaka, First principles phonon calculations in materials science, Scr. Mater. 108 (2015) 1–5, https://doi.org/10.1016/j.scriptamat.2015.07.021.

[40] F.D. Murnaghan, The compressibility of media under extreme pressures, Proc. Natl. Acad. Sci. U. S. A 30 (9) (1944) 244–247.

[41] Y. Soni, U. Rani, A. Shukla, T.K. Joshi, A. Verma, Transition metal-based halides double Cs_2ZSbX_6 (Z = Ag, Cu, and X = Cl, Br, I) perovskites: a mechanically stable and highly absorptive materials for photovoltaic devices, J. Solid State Chem. 314 (2022) 123420.

[42] N. Ahmed, et al., Experimental and theoretical study of electronic, magnetic and mechanical properties of cubic $LaMnO_3$ under extreme stress, Mater. Res. Express 6 (2019) 126123, https://doi.org/10.1088/2053-1591/ab5e04.

[43] F. Rehman, et al., Tuning the optical properties through bandgap engineering in Si-doped YAuPb: ab initio study, J. Comput. Electron. 21 (2022) 119–127, https://doi.org/10.1007/s10825-021-01845-x.

[44] J. Khan, et al., Exploring rare-earth compound $ErMn_2Si_2$ for thermoelectric and photoelectrochemical applications using density functional theory, J. Magn. Magn Mater. 600 (2024) 172156, https://doi.org/10.1016/j.jmmm.2024.172156.

[45] B. Ghebouli, M.A. Ghebouli, T. Chihi, M. Fatmi, S. Boucetta, M. Reffas, First-principles study of structural, elastic, electronic and optical properties of $SrMO_3$ (M = Ti and Sn), Solid State Commun. 149 (47–48) (2009) 2244–2249, https://doi.org/10.1016/j.ssc.2009.09.001.

[46] R. Ameur, K. Bouferrache, A. Guibadj, et al., Half-metallicity and spin-gapless semiconducting properties in FeCrTiM (M = Al, As, Si) quaternary Heusler alloys for spintronic, thermoelectric and optoelectronic applications, Adv. Compos. Hybrid Mater. 8 (2025) 366, https://doi.org/10.1007/s42114-025-01466-z.

[47] M.A. Ghebouli, T. Chihi, B. Ghebouli, M. Fatmi, Study of the structural, elastic, electronic and optical properties of lead free halide double perovskites Cs_2AgBiX_6 (X = Br, Cl), Chin. J. Phys. 56 (2018) 323–330, https://doi.org/10.1016/j.cjph.2018.01.004.

[48] F. Benlakhdar, M.A. Ghebouli, M. Fatmi, B. Ghebouli, S. Alomairy, M.J. A. Abualreish, T. Althagafi, W. Djerir, Electronic and optical properties of lead-free $K_2AgSbBr_6$ double perovskite tuned by doping elements Cu^+, Bi^{3+}, and I^-, Sci. Rep. 15 (2025) 40362, https://doi.org/10.1038/s41598-025-24417-6.

[49] K. Bouferrache, M.A. Ghebouli, M. Fatmi, G. Sheetah, S. Alomairy, M.J. A. Abualreish, A. Smerat, M. Yaylacı, Synergistic optoelectronic and thermoelectric performance in $Rb_2AsAuBr_6$ and $Rb_2AsAuCl_6$ double perovskites for multifunctional energy conversion, Sci. Rep. (2026), https://doi.org/10.1038/s41598-026-42440-z.

[50] M. Fatmi, K. Bouferrache, M.A. Ghebouli, B. Ghebouli, F.K. Alanazi, M. D. Albaqami, S. Mohammad, A. Benali, High performance double perovskites of $Cs_2InAgBr_6$ and $Cs_2InAgCl_6$ structural electronic optical and thermoelectric properties for next generation photovoltaics, Sci. Rep. 15 (2025) 20851, https://doi.org/10.1038/s41598-025-04600-5.

[51] R. Beddiaf, K. Bouzgou, H. Bouderba, H. Righi, M. Dhiaf, A. Hidoussi, Y. Djaballah, Theoretical investigation of structural, electronic, and optical features of lead-free Rb_2LiAsX_6 (X = F, Cl, Br, I) double perovskites, Physica Scripta 101 (2026) 115910, https://doi.org/10.1088/1402-4896/ae4dd0.

[52] M.E.A. Monir, H. Baltach, K. Bouferrache, M. Fatmi, M.A. Ghebouli, F.K. Alanazi, B. Ghebouli, M.I. Benamrani, R. Boudissa, Half-metallicity of novel halide double perovskites K_2CuVCl_6 and Rb_2CuVCl_6: application in next-generation spintronic devices, RSC Adv. 15 (2025) 17685–17694, https://doi.org/10.1039/D5RA02811F.

[53] B. Ghebouli, M.A. Ghebouli, H. Choutri, M. Fatmi, T. Chihi, L. Louail, A. Bouhemadou, S. Bin-Omran, R. Khenata, H. Khachai, An ab initio study of the structural, elastic, electronic, optical properties and phonons of the double perovskite oxides Sr_2AlXO_6 (X = Ta, Nb, V), Mater. Sci. Semicond. Process. 42 (2016) 405–412, https://doi.org/10.1016/j.mssp.2015.09.026.

[54] S. El Kamli, Y. Selmani, A. Jabar, L. Bahmad, A. Kassou-Ou-Ali, DFT investigation of physical properties of the double perovskites Cs_2CaMCl_6 (M = Ge or Pb), Trans. Electr. Electron. Mater. (2025), https://doi.org/10.1007/s42341-025-00672-2.